Provided for non-commercial research and education use.
Not for reproduction, distribution or commercial use.

(This is a sample cover image for this issue. The actual cover is not yet available at this time.)

This article appeared in a journal published by Elsevier. The attached copy is furnished to the author for internal non-commercial research and education use, including for instruction at the author's institution and sharing with colleagues.

Other uses, including reproduction and distribution, or selling or licensing copies, or posting to personal, institutional or third party websites are prohibited.

In most cases authors are permitted to post their version of the article (e.g. in Word or Tex form) to their personal website or institutional repository. Authors requiring further information regarding Elsevier's archiving and manuscript policies are encouraged to visit:

http://www.elsevier.com/authorsrights

Author's Personal Copy

Journal of Manufacturing Processes 25 (2017) 411–417

Contents lists available at ScienceDirect

Journal of Manufacturing Processes

journal homepage: www.elsevier.com/locate/manpro

# Influences of energy density on microstructure and consolidation of selective laser melted bismuth telluride thermoelectric powder

Ahmed El-Desouky[a], Michael Carter[a], Mohamad Mahmoudi[b], Alaa Elwany[b], Saniya LeBlanc[a,*]

[a] Department of Mechanical & Aerospace Engineering, The George Washington University, 800 22nd St. NW, Washington DC 20052, USA
[b] Department of Industrial & Systems Engineering, Texas A&M University, 3131 TAMU, College Station, TX 77843, USA

ARTICLE INFO

*Article history:*
Received 5 October 2016
Accepted 6 December 2016

*Keywords:*
Selective laser melting
Thermoelectrics
Bismuth telluride

ABSTRACT

Selective laser melting is a well-established additive manufacturing technique for metals and ceramics, and there is significant interest in expanding the manufacturing capability of this technique by enabling processing of more materials. Notably, selective laser melting has not been demonstrated on semiconducting materials which are significant for energy conversion technologies. Thermoelectric materials are semiconductors that can convert heat into electrical power. The traditional thermoelectric manufacturing process involves many assembly and machining steps which lead to material losses, added time and cost, and performance degradation. Utilizing selective laser melting in the manufacturing of thermoelectric modules can minimize assembly steps and eliminate machining processes. In this study, a standard bismuth telluride thermoelectric powder was processed for the first time in a commercial Prox™ 100 selective laser melting system under different energy densities. The surfaces of $Bi_2Te_3$ specimens were successfully melted under all processing conditions, and the entire thickness of specimens processed at higher laser power inputs was mostly melted. The increase in laser power also reduced the presence of porosities on the surface of the specimens. However, cross-sectional examination showed that internal pores were present within the molten region and at the interface between the molten region and the unmelted powder under all investigated laser power inputs. The consistency of these results with early results for select laser melting of metals demonstrates the promise for expanding the materials processing capabilities of this additive manufacturing technique.

© 2016 The Society of Manufacturing Engineers. Published by Elsevier Ltd. All rights reserved.

## 1. Introduction

Thermoelectric devices convert waste heat into electrical power, creating opportunities for waste heat recovery in high-temperature systems from industrial power plants to automobiles [1,2]. A thermoelectric device typically consists of multiple junctions of n- and p-type semiconducting thermoelectric legs. The legs are connected electrically in series and thermally in parallel as shown in Fig. 1. When a temperature gradient is applied across the thermoelectric material, electric charge carriers move from the hot side to the cold side, ultimately resulting in a voltage drop—a phenomenon known as the Seebeck effect.

The performance of a thermoelectric material is evaluated through the dimensionless figure of merit $ZT = \left(S^2\sigma/k\right)T$, where $S$ is the Seebeck coefficient, $\sigma$ is the electrical conductivity, $k$ is the thermal conductivity, and $T$ is the absolute temperature. A material with good thermoelectric properties has a high Seebeck coefficient, high electrical conductivity, and low thermal conductivity to maintain the temperature gradient across the material. Chalcogenide materials are commonly used in thermoelectric devices that operate over a wide range of operating temperatures (100–1000 K) [3,4]. Bismuth telluride ($Bi_2Te_3$) and its solid solutions are among the most commonly used chalcogenides in off-the-shelf thermoelectric devices operating near room temperature [3,5,6]. Although noteworthy progress in enhancing the thermoelectric properties of $Bi_2Te_3$ and its alloys through microstructural and compositional changes has been recently reported [7–10], challenges related to device manufacturing and assembly continue to slow the progress of thermoelectric power generation [4,11].

* Corresponding author at: The George Washington University, Department of Mechanical & Aerospace Engineering, 800 22nd St. NW, Suite 3000, Washington, DC 20052, USA.
*E-mail addresses:* ahmed.eldesouky@gmail.com (A. El-Desouky), mjcarter@gwu.edu (M. Carter), mmahmoudi@tamu.edu (M. Mahmoudi), elwany@tamu.edu (A. Elwany), sleblanc@gwu.edu (S. LeBlanc).

http://dx.doi.org/10.1016/j.jmapro.2016.12.008
1526-6125/© 2016 The Society of Manufacturing Engineers. Published by Elsevier Ltd. All rights reserved.

Author's Personal Copy



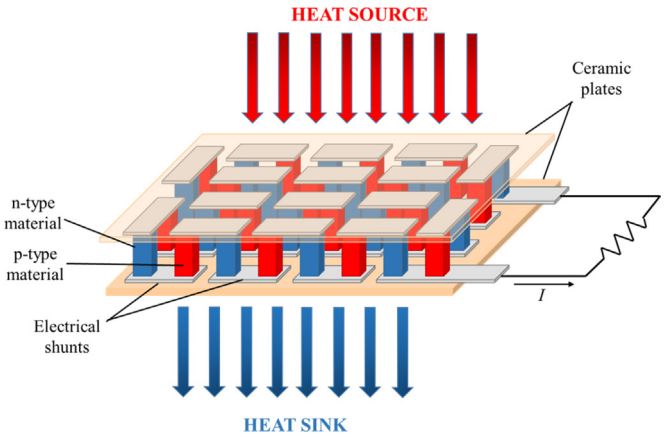


**Fig. 1.** Schematic of a thermoelectric device showing multiple n- and p-type leg couples connected electrically in series and thermally in parallel. A typical thermoelectric device can consist of hundreds of legs.

The traditional thermoelectric device manufacturing process involves multiple steps including processing and assembly. First, the constituents of the thermoelectric compound are alloyed using mechanical milling processes. The alloyed powder is then consolidated through methods such as hot pressing or spark plasma sintering. The resulting ingots are diced into the leg shape, and finally the legs are generally picked and placed into the final assembly. In contrast, additive manufacturing represents an attractive manufacturing alternative for thermoelectric devices. A recent workshop by the U.S. Department of Energy indicates that labor accounts for a significant portion of the cost of these devices [12]. Additive manufacturing technologies such as selective laser melting (SLM) are capable of producing 3-dimensional objects directly from a digital CAD model [13] without the need for customized tooling or manual assembly. This capability can potentially be leveraged to eliminate the assembly of many components and reduce the time and cost involved in producing complex thermoelectric modules. For example, Crane et al. [14] present a simulation case study using a prototype thermoelectric system to highlight the potential capability of additive manufacturing in automated self-assembly and integration. Co-authors of this work recently provided an overview of challenges in thermoelectric device manufacturing and highlighted the potential of additive manufacturing technologies in thermoelectric materials processing [15].

Selective laser melting (SLM) has been used in numerous studies in the literature to produce complex customized parts from metallic materials and alloys including stainless steels [16–20], titanium alloys [21–24], and nickel-based super alloys [25–28] among others. Preliminary findings on the formation of single melt tracks of $Bi_2Te_3$ powder compacts using a low repetition pulsed laser [29,30,15] were previously reported. In the current work, an initial investigation is conducted on the full consolidation of bismuth telluride ($Bi_2Te_3$) powder using SLM. $Bi_2Te_3$ powder is the only commercially available thermoelectric pre-alloyed powder. Off-the-shelf $Bi_2Te_3$ powder lacks the physical characteristics that would allow it to spread into sequential thin layers which is essential for the SLM process. The irregular shape of the particles and the large particle size distribution (visible in Fig. 2) result in increased friction between the particles and leads to poor flowability and spreadability of the powder. This initial investigation is focused on processing $Bi_2Te_3$ in powder compact form primarily to provide insight into the effect of laser energy density on the microstructural evolution and densification behavior of laser-irradiated $Bi_2Te_3$. These insights will serve as a foundation to enable subsequent layer-by-layer SLM processing of thermoelectric modules.

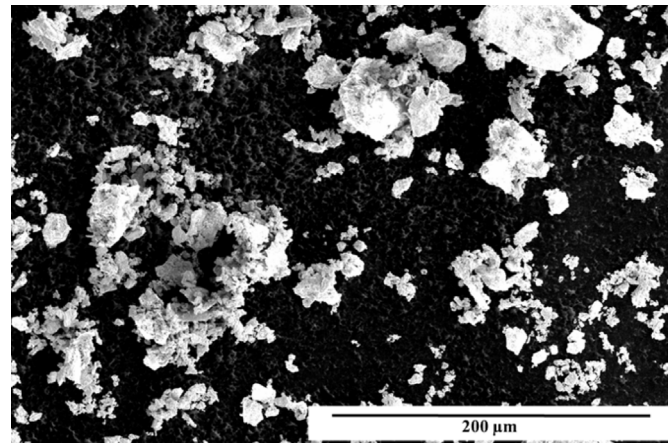


**Fig. 2.** Scanning electron micrograph of off-the-shelf $Bi_2Te_3$ powder.

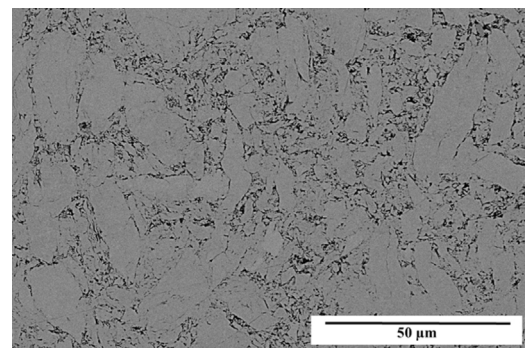


**Fig. 3.** Scanning electron micrograph of a polished cross-section of a $Bi_2Te_3$ powder compact.

**Table 1**
Selective laser melting processing parameters for the 16 powder compacts processed in a ProX100.

| Specimens | Power (W) | Speed (mm/s) | Energy density (J/mm$^2$) |
|---|---|---|---|
| 1–4 | 10 | 350 | 0.57 |
| 5–8 | 15 | 350 | 0.86 |
| 9–12 | 20 | 350 | 1.14 |
| 13–16 | 25 | 350 | 1.42 |

## 2. Experiments

$Bi_2Te_3$ powder (−325 mesh, 99.99% trace metals basis, Sigma Aldrich) was compacted using a hydraulic press and a hardened steel 6 mm die. The final compacts are 6 mm diameter and ~500 μm thick. Fig. 3 shows a scanning electron micrograph of a representative $Bi_2Te_3$ powder compact used in this study. Next, the powder compacts were processed on a commercial ProX$^{TM}$ 100 SLM system. The ProX$^{TM}$ 100 uses a 50-W fiber laser with a Gaussian profile and approximately 100 μm spot size to selectively melt metallic powder in a 3.94 × 3.94 × 3.15 in. build envelope. This study is the first of its kind in processing thermoelectric powder on this SLM system.

The powder compacts were placed on the build plane and processed under an argon atmosphere with the oxygen level kept below 700 ppm. Sixteen specimens in total were processed. The scanning speed of the laser and the hatch distance were kept constant at 350 mm/s and 70 μm, respectively, and the laser energy density was varied by adjusting the laser power as shown in Table 1.

For subsurface analyses, the specimens were cleaved normal to the build direction. The specimens were then cast in epoxy resin, and an Allied High Tech Multiprep polishing unit was used to grind and polish the cross-sectional surface down to 0.04 μm

Author's Personal Copy



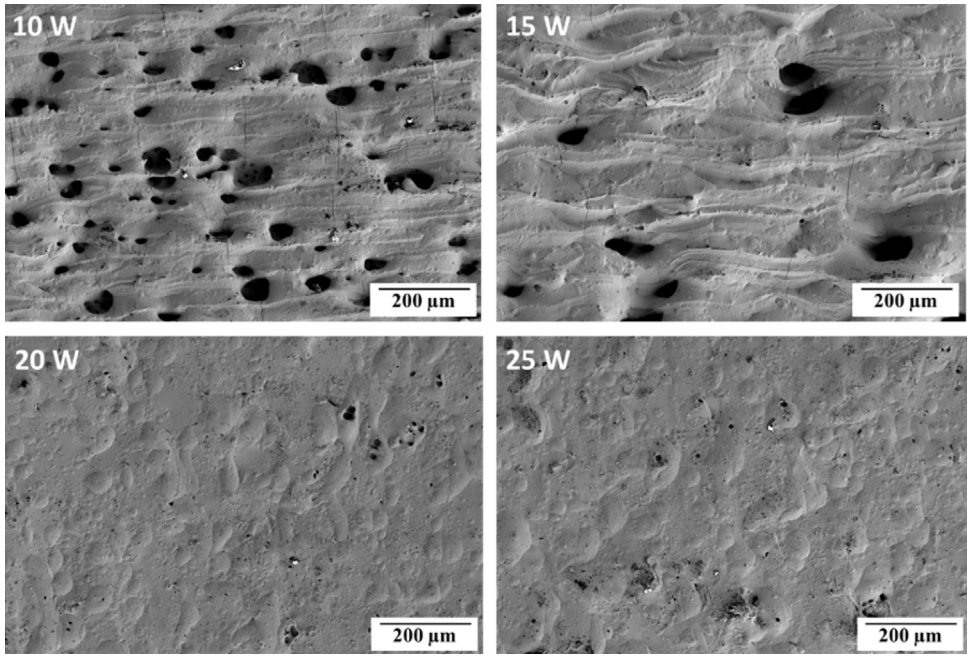


**Fig. 4.** SEM micrographs taken of the top surface of the SLM-processed $Bi_2Te_3$ powder compacts showing surface porosity decrease with the increase in laser power input.

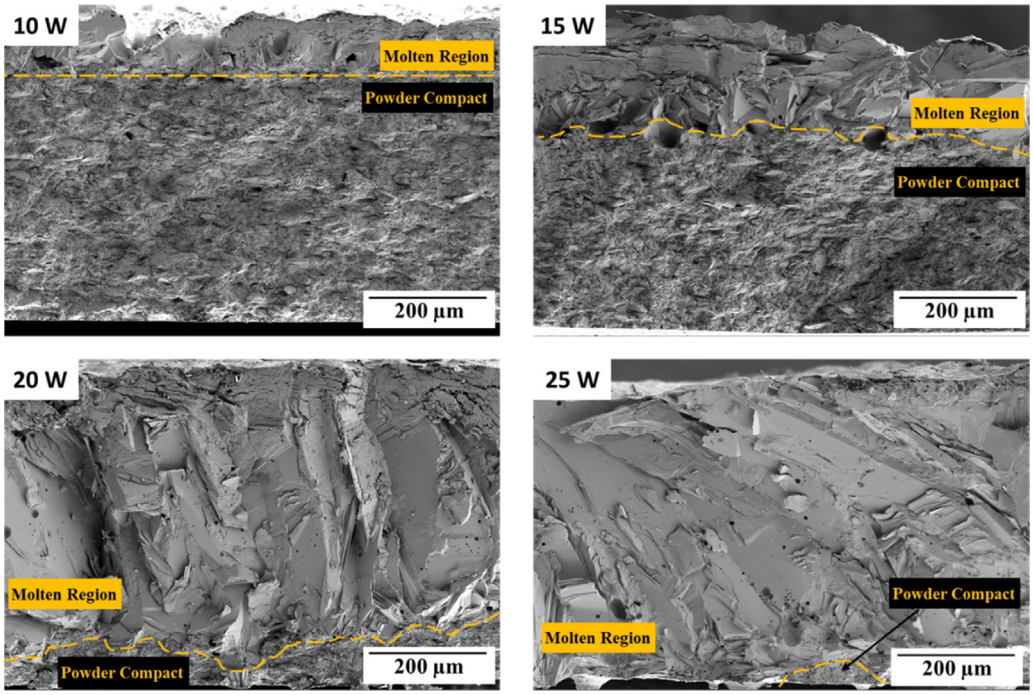


**Fig. 5.** Cross-sectional scanning electron fractographs of $Bi_2Te_3$ powder compacts processed with laser powers 10–25 W showing the depth of the melt zone for each laser power input setting.

finish. A Leica DM2700 M RL optical microscope equipped with a light polarizer was used for microstructural observation. Densification depth and porosity content were evaluated using a FEI Teneo LV scanning electron microscope. A Rigaku Miniflex II Cu–Kα X-ray diffractometer was used for phase identification in the SLM-processed specimens. The processed specimens were first gently crushed into powder using mortar and pestle to alleviate preferred crystallographic orientations.

## 3. Results and discussion

Fig. 4 shows SEM micrographs taken of the top surface of the laser-processed $Bi_2Te_3$ powder compacts. A large amount of homogeneously distributed porosity is observed on the surface of specimens processed at 10 W. The porosity content decreases with the increase in laser power, and at the higher power settings the average size of the surface pores also decreases. Cross-sectional examination of the fractured surface of the processed powder reveals that the depth of melt increases with the increase in laser

Author's Personal Copy



power (Fig. 5). At 10 W and 15 W, the powder compacts are only partially melted at depths of ~80 μm and ~180 μm, respectively. Specimens processed at the higher power settings are almost completely melted with scattered unconsolidated regions at the bottom of the specimens. The large increase in molten depth observed in the powder compacts processed at higher laser powers may be explained by the exponential dependence of recoil pressure on surface temperature. The high laser intensities associated with SLM can drive strong evaporation at the surface of the molten region [31,32]. Evaporation and collisions from re-condensing particles give rise to a back-pressure on the free surface of the molten pool, termed recoil pressure [33]. Analytically, recoil pressure has been shown to increase exponentially with increasing surface temperature [34].

Randomly oriented river lines are observed on the fracture surface indicating a transgranular fracture mode which is common in brittle materials with lamellar crystallographic structures such as bismuth telluride (Fig. 6) [35]. Optical micrographs of the polished cross-section with polarized light are used for microstructural examination. Fig. 7 shows the microstructural evolution of $Bi_2Te_3$ powder processed with different laser power inputs. At higher power settings the shape of the grains is elongated in a direction normal to the build direction. The formation of grains with similar shape and orientation is common in SLM of metals and has been reported by Niendorf et al. [37] and Kanagarajah et al. [26].

Fig. 8 shows scanning electron micrographs of the $Bi_2Te_3$ specimens sintered under different laser powers. Two different types of porosity are observed below the surface of the molten region. At the higher power settings (20 W and 25 W), spherical shaped pores are observed across the thickness of the molten region, while more irregularly shaped pores are present at the interface between the molten region and the powder compact for all specimens. Spherical pores generally result from trapped gases in the molten pool [38,39]. Pre-existing closed pore structures in the original green compacts act as initiation sites for gas porosity formation [40]. During laser melting of the powder, small pores will collapse under the high surface tension of the molten pool, while larger pores will overcome the surface tension. Trapped gases in the form of bubbles will remain trapped in the molten pool due to the extremely rapid solidification rates experienced in SLM. Another possible explanation for the spherical pores observed at higher power settings is keyhole instability and collapse, which can lead to trapped gases, bubble formation and porosity upon solidification. Notably, this has been observed in deep penetration laser welding at low speeds [41,42]. On the other hand, irregular pores are generally present at the melt pool boundaries and could be a result of unmelted powder or shrinkage at the interface between the molten pool and the unconsolidated powder.

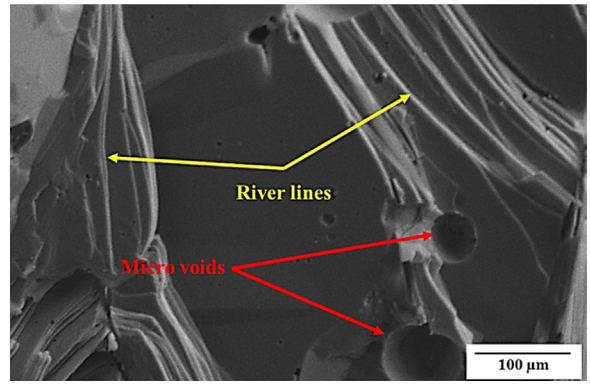


**Fig. 6.** Scanning electron fractographs of the melt zone of a specimen processed at 20 W laser power, showing microvoids (indicated by red arrows) and transgranular river patterns (yellow arrows) on the fracture surface. (For interpretation of the references to colour in this figure legend, the reader is referred to the web version of this article.)

The phase purity of the SLM processed $Bi_2Te_3$ specimens is identified using XRD (Fig. 9). For all laser processing conditions in

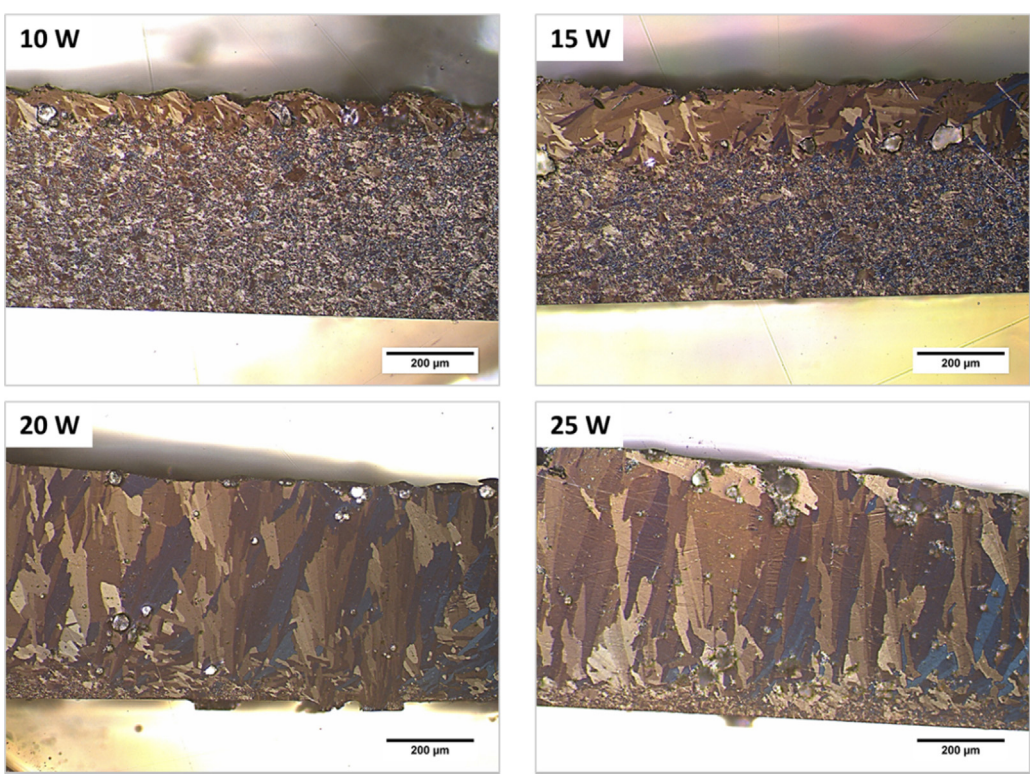


**Fig. 7.** Polarized light microscope images of the cross-sectional surface of $Bi_2Te_3$ samples processed at different laser power inputs showing elongated microstructures.

Author's Personal Copy



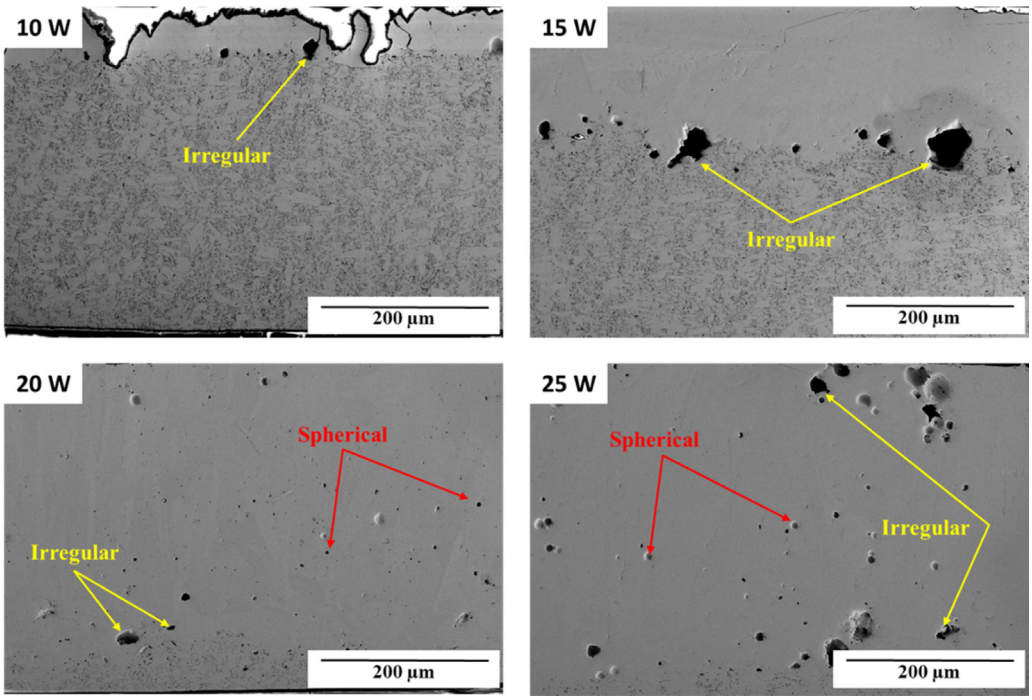


**Fig. 8.** SEM micrographs of the cross-sectional surface of $Bi_2Te_3$ samples processed at different laser power inputs showing spherical pores (indicated by red arrows) and irregulare shaped pores (indicated by yellow arrows). (For interpretation of the references to colour in this figure legend, the reader is referred to the web version of this article.)

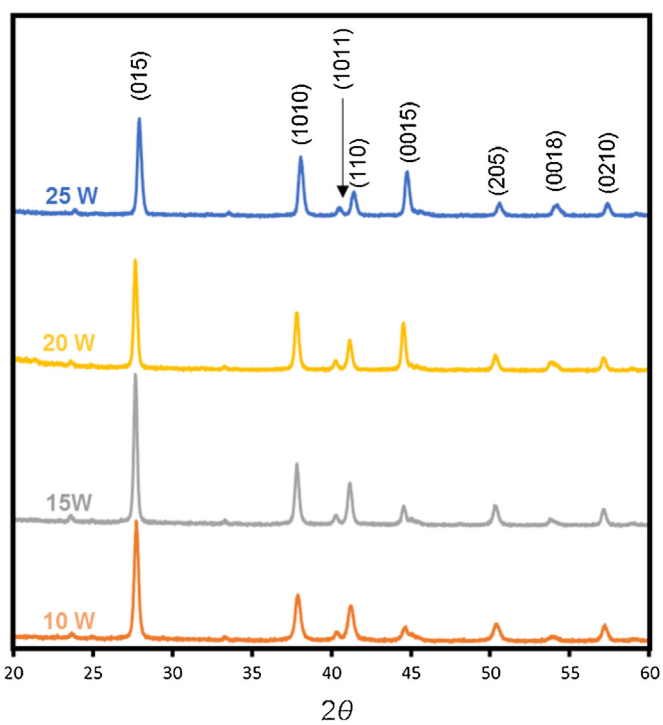


**Fig. 9.** X-ray diffraction patterns of $Bi_2Te_3$ powder compacts processed with laser powers 10–25 W.

this study, the XRD patterns are well-matched with binary $Bi_2Te_3$ (PDF#15-0863) indicating that no new phases were formed during SLM. The relative intensities of the (0015) and (0018) planes are clearly stronger for specimens processed at 20 W and 25 W laser powers. Systematic variation in diffraction peak intensities indicates preferred orientation of crystallites in the powder sample [43]. The presence of large, elongated crystallites in the 20 W and 25 W processed specimens makes it difficult for the crushed powder to adopt a random orientation. Preferred crystallographic orientation is not evident in the XRD patterns of the specimens processed at lower power settings due to the presence of a large percentage of unconsolidated powder in the specimen. Any preferred orientation that may have been present in the partial molten region would have been masked by the randomly oriented grains in the unconsolidated region. Changes in peak intensities resulting from crystallographic preferred orientations were previously reported for $Bi_2Te_3$ powder processed with spark plasma sintering, rolling, and forging [6,44,45]. Formation of preferred crystallographic orientation during processing of $Bi_2Te_3$ was also found to influence anisotropy of thermoelectric properties.

## 4. Conclusion

The results presented here are a unique demonstration of selective laser melting of a thermoelectric material. Selective laser melting of $Bi_2Te_3$ thermoelectric powder was investigated on a commercial SLM system (ProX$^{TM}$ 100) under variable energy densities. Powder compacts were used for the investigation since commercially available $Bi_2Te_3$ powder lacks sufficient flowability and spreadability for layer-by-layer manufacturing. Results show that the depth of the melt region in SLM-processed compacts increases with an increase in laser power, and the specimens were almost completely melted at the higher power settings (20 W and 25 W). Surface porosities were found to decrease significantly with the increase in energy density. However, for all processing conditions, subsurface pores were present due to trapped gases and shrinkage at the melt pool boundaries. X-ray diffraction phase analysis shows that no new phases were formed under all investigated processing conditions. The results from the current study provide a foundation for future work in investigating the manufacturability of $Bi_2Te_3$ in a layer-by-layer fashion using SLM. The use of additive manufacturing can potentially provide an attractive alternative

Author's Personal Copy



to traditional manufacturing in the fabrication of thermoelectric devices.

## Acknowledgements

The authors wish to thank The George Washington University Nanofabrication and Imaging Center for its support of the scanning electron microscopy work and the Wagner Lab for its help with XRD analysis.

## References

[1] Tritt TM. Thermoelectric phenomena, materials, and applications. Annu Rev Mater Res 2011;41:433–48, http://dx.doi.org/10.1146/annurev-matsci-062910-100453.
[2] Martín-González M, Caballero-Calero O, Díaz-Chao P. Nanoengineering thermoelectrics for 21st century: energy harvesting and other trends in the field. Renew Sustain Energy Rev 2013;24:288–305, http://dx.doi.org/10.1016/j.rser.2013.03.008.
[3] Madavali B, Kim H, Hong S. Effect of chemical composition on the thermoelectric properties of n-type $Bi_2Te_3$ alloys fabricated by gas atomization and hot extrusion. J Electron Mater 2014;43:2390–6, http://dx.doi.org/10.1007/s11664-014-3077-6.
[4] LeBlanc S. Thermoelectric generators: linking material properties and systems engineering for waste heat recovery applications. Sustain Mater Technol 2014;1–2:26–35, http://dx.doi.org/10.1016/j.susmat.2014.11.002.
[5] Kim KT, Lim TS, Ha GH. Improvement in thermoelectric properties of n-type bismuth telluride nanopowders by hydrogen reduction treatment. Rev Adv Mater Sci 2011;28:196–9.
[6] Zhao LD, Zhang B, Li J, Zhang HL, Liu WS. Enhanced thermoelectric and mechanical properties in textured n-type $Bi_2Te_3$ prepared by spark plasma sintering. Solid State Sci 2008;10, http://dx.doi.org/10.1016/j.solidstatesciences.2007.10.022.
[7] Hochbaum AI, Chen R, Delgado RD, Liang W, Garnett EC, Najarian M, et al. Enhanced thermoelectric performance of rough silicon nanowires. Nature 2008;451:163–7, http://dx.doi.org/10.1038/nature06381.
[8] Shi X, Yang J, Salvador JR, Chi M, Cho JY, Wang H, et al. Multiple-filled skutterudites: high thermoelectric figure of merit through separately optimizing electrical and thermal transports. J Am Chem Soc 2011;133:7837–46, http://dx.doi.org/10.1021/ja111199y.
[9] Biswas K, He J, Blum ID, Wu C-I, Hogan TP, Seidman DN, et al. High-performance bulk thermoelectrics with all-scale hierarchical architectures. Nature 2012;489:414–8, http://dx.doi.org/10.1038/nature11439.
[10] Poudel B, Hao Q, Ma Y, Lan Y, Minnich A, Yu B, et al. High-thermoelectric performance of nanostructured bismuth antimony telluride bulk alloys. Science 2008;320(5876):634–8, http://dx.doi.org/10.1126/science.1156446.
[11] Zebarjadi M, Esfarjani K, Dresselhaus MS, Ren ZF, Chen G. Perspectives on thermoelectrics: from fundamentals to device applications. Energy Environ Sci 2012;5:5147–62, http://dx.doi.org/10.1039/C1EE02497C.
[12] Department of Energy, 2015 Quadrennial technology review, 2015.
[13] ASTM, F2792. 2012 Standard terminology for additive manufacturing technologies. 2012.
[14] Crane NB, Tuckerman J, Nielson GN. Self-assembly in additive manufacturing: opportunities and obstacles. Rapid Prototyp J 2011;17:211–7, http://dx.doi.org/10.1108/13552541111124798.
[15] El-Desouky A, Carter M, Andre MA, Bardet PM, LeBlanc S. Rapid processing and assembly of semiconductor thermoelectric materials for energy conversion devices. Mater Lett 2016, http://dx.doi.org/10.1016/j.matlet.2016.07.152.
[16] Rafi HK, Pal D, Patil N, Starr TL, Stucker BE. Microstructure and mechanical behavior of 17-4 precipitation hardenable steel processed by selective laser melting. J Mater Eng Perform 2014;23:4421–8.
[17] Riemer A, Leuders S, Thöne M, Richard HA, Tröster T, Niendorf T. On the fatigue crack growth behavior in 316L stainless steel manufactured by selective laser melting. Eng Fract Mech 2014;120:15–25.
[18] Murr LE, Gaytan SM, Ramirez DA, Martinez E, Hernandez J, Amato KN, et al. Metal fabrication by additive manufacturing using laser and electron beam melting technologies. J Mater Sci Technol 2012;28:1–14.
[19] Averyanova M, Bertrand PH, Verquin B. Studying the influence of initial powder characteristics on the properties of final parts manufactured by the selective laser melting technology: a detailed study on the influence of the initial properties of various martensitic stainless steel powders on. Virtual Phys Prototyp 2011;6:215–23.
[20] Averyanova M, Cicala E, Bertrand P, Grevey D. Experimental design approach to optimize selective laser melting of martensitic 17-4 PH powder: part I-single laser tracks and first layer. Rapid Prototyp J 2012;18:28–37.
[21] Song B, Dong S, Zhang B, Liao H, Coddet C. Effects of processing parameters on microstructure and mechanical property of selective laser melted $Ti_6Al_4V$. Mater Des 2012;35:120–5.
[22] Gu DD, Meiners W, Wissenbach K, Poprawe R. Laser additive manufacturing of metallic components: materials, processes and mechanisms. Int Mater Rev 2012;57:133–64, http://dx.doi.org/10.1179/1743280411Y.0000000014.
[23] Leuders S, Thöne M, Riemer A, Niendorf T, Tröster T, Richard HA, et al. On the mechanical behaviour of titanium alloy $TiAl_6V_4$ manufactured by selective laser melting: fatigue resistance and crack growth performance. Int J Fatigue 2013;48:300–7.
[24] Vrancken B, Thijs L, Kruth J-P, Van Humbeeck J. Heat treatment of $Ti_6Al_4V$ produced by selective laser melting: microstructure and mechanical properties. J Alloys Compd 2012;541:177–85.
[25] Wang Z, Guan K, Gao M, Li X, Chen X, Zeng X. The microstructure and mechanical properties of deposited-IN718 by selective laser melting. J Alloys Compd 2012;513:518–23.
[26] Kanagarajah P, Brenne F, Niendorf T, Maier HJ. Inconel 939 processed by selective laser melting: effect of microstructure and temperature on the mechanical properties under static and cyclic loading. Mater Sci Eng A 2013;588:188–95.
[27] Amato KN, Gaytan SM, Murr LE, Martinez E, Shindo PW, Hernandez J, et al. Microstructures and mechanical behavior of Inconel 718 fabricated by selective laser melting. ACTA Mater 2012;60:2229–39.
[28] Jia Q, Gu D. Selective laser melting additive manufacturing of Inconel 718 superalloy parts: densification, microstructure and properties. J Alloys Compd 2014;585:713–21.
[29] Leblanc S, El-Desouky A. Thermoelectric material and device formation with laser sintering and melting. 2015;62/164:335.
[30] El-Desouky A, Read A, Bardet P, Andre M, LeBlanc S. Selective laser melting of a bismuth telluride thermoelectric material. Proc Solid Free Symp 2015:1043–50.
[31] King WE, Anderson AT, Ferencz RM, Hodge NE, Kamath C, Khairallah SA, et al. Laser powder bed fusion additive manufacturing of metals; physics, computational, and materials challenges. Appl Phys Rev 2015;2:041304, http://dx.doi.org/10.1063/1.4937809.
[32] Klassen A, Scharowsky T, Körner C. Evaporation model for beam based additive manufacturing using free surface lattice Boltzmann methods. J Phys D Appl Phys 2014;47:275303, http://dx.doi.org/10.1088/0022-3727/47/27/275303.
[33] Knight CJ. Theoretical modeling of rapid surface vaporization with back pressure. AIAA J 1979;17:519–23, http://dx.doi.org/10.2514/3.61164.
[34] Anisimov SI. Vaporization of metal absorbing laser radiation. Sov Phys JETP 1968;27:182–3.
[35] ASM Handbook Volume 11, Failure Analysis and Prevention (ASM International). 2002, 559–586.
[37] Niendorf T, Leuders S, Riemer A, Richard HA, Tröster T, Schwarze D. Highly anisotropic steel processed by selective laser melting. Metall Mater Trans B Process Metall Mater Process Sci 2013;44:794–6, http://dx.doi.org/10.1007/s11663-013-9875-z.
[38] Monroy K, Delgado J, Ciurana J. Study of the pore formation on CoCrMo alloys by selective laser melting manufacturing process. Procedia Eng 2013;63:361–9, http://dx.doi.org/10.1016/j.proeng.2013.08.227.
[39] Kempen K, Thijs L, Yasa E, Badrossamay M, Verheecke W, Kruth J-P. Process optimization and microstructural analysis for selective laser melting of AlSi10Mg. Solid Free Fabr Symp 2011;22:484–95.
[40] Cao X, Jahazi M, Immarigeon JP, Wallace W. A review of laser welding techniques for magnesium alloys. J Mater Process Technol 2006;171:188–204, http://dx.doi.org/10.1016/j.jmatprotec.2005.06.068.
[41] Katayama S, Kawahito Y, Mizutani M. Elucidation of laser welding phenomena and factors affecting weld penetration and welding defects. Phys Procedia 2010;5:9–17, http://dx.doi.org/10.1016/j.phpro.2010.08.024.
[42] Courtois M, Carin M, Le P, Lee JY, Ko SH, Farson DF. et al. Mechanism of keyhole formation and stability in stationary laser welding. J. Phys. D: Appl. Phys 2002;35:1570.
[43] Suryanarayana C, Norton MG. X-ray diffraction. Boston, MA: Springer US; 1998, http://dx.doi.org/10.1007/978-1-4899-0148-4.
[44] Saleemi M, Toprak MS, Li S, Johnsson M, Muhammed M. Synthesis, processing, and thermoelectric properties of bulk nanostructured bismuth telluride ($Bi_2Te_3$). J Mater Chem 2012;22:725, http://dx.doi.org/10.1039/c1jm13880d.
[45] Euvananont C, Jantaping N, Thanachayanont C. Effects of composition and preferred orientation on microstructure and thermoelectric properties of p-type $(Bi_xSb_{(1-x)})_2Te_3$ alloys. Curr Appl Phys 2011;11:S246–50, http://dx.doi.org/10.1016/j.cap.2010.11.011.

**Dr. Ahmed El Desouky** is a postdoctoral scientist in the Department of Mechanical and Aerospace Engineering at The George Washington University. His research interests are in advanced materials processing methods and powder metallurgical processes with specific emphasis on additive manufacturing applications. Dr. El Desouky obtained a Ph.D. in Engineering Sciences (Mechanical and Aerospace Engineering) from the University of California, San Diego (joint with San Diego State University) and a B.Sc. in Production Engineering from Alexandria University, Egypt.

**Michael Carter** received his B.S. in Mechanical Engineering from the University of Maryland, College Park, and his M.S. in Mechanical and Aerospace Engineering from The George Washington University. His research work at The George Washington University focused on laser processing of thermoelectric materials. He is currently a graduate student at Columbia University in the Department of Applied Physics and Applied Mathematics working toward a Ph.D. in Materials Science and Engineering.

**Mohamad Mahmoudi** received his B.S. degree in Mechanical Engineering from University of Tehran, Tehran, Iran, and his M.S. degree in Industrial Engineering from

Author's Personal Copy



Iran University of Science and Technology, Tehran, Iran. He is currently a graduate student with the Department of Industrial & Systems Engineering, Texas A&M University, working toward the Ph.D. degree in Industrial Engineering. His research interests are monitoring methods, experimental design, and characterization of parts for additive manufacturing processes.

**Dr. Alaa Elwany** is an assistant professor at the Department of Industrial & Systems Engineering, Texas A&M University. He received his B.Sc. and M.Sc. degrees in Production and Industrial Engineering, respectively, from Alexandria University, Egypt and his Ph.D. in Industrial & Systems Engineering from Georgia Institute of Technology, USA in 2009. His research interests are in the modeling, analysis, and control in advanced manufacturing processes with particular emphasis on Additive Manufacturing processes.

**Dr. Saniya LeBlanc** is an assistant professor in the Department of Mechanical and Aerospace Engineering at The George Washington University. She uses scalable manufacturing techniques to create materials and devices for energy applications. Previously, she was at Alphabet Energy where she created research, development, and manufacturing solutions for thermoelectric technologies and evaluated new power generation materials. Dr. LeBlanc obtained an MS and PhD in mechanical engineering at Stanford University and a BS from Georgia Institute of Technology.